Environmental Fluid Mechanics manuscript No. EFMC-D-13-00004
DOI: 10.1007/s10652-013-9302-7

A simplified approach to address turbulence modulation in turbidity currents as a response to slope breaks and loss of lateral confinement

Mariano I. Cantero · S. Balachandar · Alessandro Cantelli · Gary Parker

Received: January 4, 2013 / Accepted: July 28, 2013

Abstract Turbidity currents traversing canyon-fan systems flow over bed slopes that decrease in the downstream direction. This slope decrease eventually causes turbidity currents to decelerate and enter a net-depositional mode. When the slope decrease is relatively rapid in the downstream direction, the turbidity current undergoes a concomitantly rapid and substantial transition. Similar conditions are found when turbidity currents debouch to fan systems with loss of lateral confinement. In this work a simplified approach to perform direct numerical simulation (DNS) of continuous turbidity currents undergoing slope breaks and loss of lateral confinement is presented and applied to study turbulence modulation in the flow. The presence of settling sediment particles breaks the top-bottom symmetry of the flow, with a tendency to self-stratify. This self-stratification damps turbulence, particularly near the bottom wall, affecting substantially the flow's ability to transport sediment in suspension. This work reports results on two different situations: turbidity currents driven by fine and coarser sediment flowing through a decreasing slope. In the case of fine sediment, after the reduction in the slope of the channel, the flow remains turbulent with only a modest influence on turbulence

M. Cantero
National Council of Scientific and Technical Research (CONICET) and Institute Balseiro, Bariloche Atomic Center, San Carlos de Bariloche, Río Negro, Argentina
Tel.: +54-294-4445100 - int 5419
E-mail: mcantero@cab.cnea.gov.ar

S. Balachandar
Department of Mechanical and Aerospace Engineering, University of Florida, Gainesville, Florida, USA
E-mail: bala1s@ufl.edu

Alessandro Cantelli
Shell International Exploration and Production, Houston, Texas, USA
E-mail: alessandro.cantelli@shell.com

Gary Parker
Department Civil and Environmental Engineering and Department of Geology, University of Illinois at Urbana-Champaign, Urbana, Illinois, USA
E-mail: parkerg@illinois.edu

statistics. In the case of coarse sediments, after the change in slope, turbulence is totally suppressed.

Keywords Turbidity currents · Turbulence modulation · Sediment transport · Direct numerical simulation

1 Introduction

Turbidity currents are flows driven by sediment in suspension (Allen, 1985; García, 1992). In these types of flows gravity acts to pull the sediment in suspension downslope, and the sediment drags the fluid along with it, so driving the current. Suspended sediment particles tend to settle down creating a vertical profile with concentration declining in the upward direction thus self-stratifying the flow. These density gradients are capable of damping turbulence (Turner, 1973; Stacey and Bowen, 1988a,b; Armenio and Sarkar, 2002) consequently reducing the ability of turbidity currents to transport sediment in suspension. If the level of turbulence is high enough to overcome sediment depositional fluxes, turbidity currents can be sustained over long periods of time transporting large amounts of sediment for long distances (Pirmez and Imran, 2003).

Turbidity currents are known to be one of the main mechanisms for sediment transport into deep ocean and for the emplacement of large scale sedimentary deposits (turbidities) (Talling et al, 2007). Many if not most of the turbidities observed in outcrops and in seismic data are associated with decelerating turbidity currents (Amy et al, 2005). When these flows traverse canyon-fan systems they flow over bed slopes that decrease in the downstream direction, either gradually (upward-concave profile) or suddenly/cyclically (e.g. stepped profile). This decrease in bed slope reduces the streamwise component of the driving force (owing to the suspended sediment) eventually causing the turbidity current to decelerate and enter a net-depositional mode (Cantero et al, 2012). When the slope decrease in the downstream direction is above a threshold value, the turbidity current may undergo a rapid and substantial transition. Similar conditions are found when turbidity currents debouch to fan systems with loss of lateral confinement. The internal structure of the deposit is completely dictated by the way sediment deposition occurs.

Lock-exchange gravity and turbidity currents have been successfully studied with direct numerical simulation (DNS) (see for example Härtel et al, 2000; Necker et al, 2005; Cantero et al, 2007a,b, 2008b). Recently, Cantero et al (2009a) have presented a simplified approach for the simulation of continuous turbidity currents. This simplified model replaces the upper boundary of the turbidity current (interface in figure 1) with a roof, so preventing ambient water entrainment and creating a channel flow. This model has been called *turbidity current with a roof* (TCR) (Cantero et al, 2009a). The flow within the channel is driven purely by the presence of sediment in the water and the only driving force in the system is the excess density of the water-sediment mixture. The channel is assumed to be adjusted so that the flow and sediment transport entering the channel equal that exiting the channel (periodic boundary conditions) (see details in Cantero et al, 2009a) providing a configuration without inflows/outflows which simplifies the implementation of the DNS model. Were the sediment to settle out completely, the

flow would cease. The TCR model thus retains a key element of turbidity currents, i.e. that they are sediment-driven. On the other hand, it simplifies the problem by allowing the possibility of a mean flow equilibrium state that varies neither in time nor in the downstream direction.

The present work extends the work of Cantero et al (2009a) to explore how the turbulence structure of a turbidity current is modified after the deceleration of the flow owing to a bed slope break or to the loss of lateral confinement (see figure 1). The following section presents the conceptualization of the problem with the TCR paradigm for DNS of continuous turbidity currents.

2 Problem setting

The TCR model for continuous turbidity currents consists of a periodic channel with zero net pressure gradient such that in the absence of sediment particles the flow is stagnant. A schematic of the setting is shown in figure 1 (see for example TCR_2 in this figure). The channel forms an angle θ with the horizontal direction and extends $L_z = H$, $L_x = 2\,\pi\,H$ and $L_y = 2\,\pi\,H/3$ in the wall-normal, streamwise and spanwise directions, respectively.

In a coordinate system attached to the channel bottom wall, the dimensionless equations that govern the flow are (Cantero et al, 2008a, 2009a)

$$\frac{\partial \tilde{\mathbf{u}}}{\partial \tilde{t}} + \tilde{\mathbf{u}} \cdot \nabla \tilde{\mathbf{u}} = -\nabla \hat{p} + \frac{1}{Re_\tau} \nabla^2 \tilde{\mathbf{u}} + \tilde{\mathbf{C}}_g \,, \tag{1}$$

$$\nabla \cdot \tilde{\mathbf{u}} = 0 \,, \tag{2}$$

$$\frac{\partial \tilde{c}}{\partial \tilde{t}} + \left(\tilde{\mathbf{u}} + \tilde{\mathbf{V}}\right) \cdot \nabla \tilde{c} = \frac{1}{Re_\tau\, Sc} \nabla^2 \tilde{c} \,, \tag{3}$$

where $\tilde{\mathbf{u}} = (\tilde{u}, \tilde{v}, \tilde{w}) = (\tilde{u}_x, \tilde{u}_y, \tilde{u}_z)$ is the dimensionless fluid velocity, $\tilde{c}$ is the dimensionless volumetric concentration of sediment, $\tilde{\mathbf{V}} = \tilde{V}(\sin\theta, 0, -\cos\theta)$ is the dimensionless settling velocity of the sediment particles with $\tilde{V}$ its magnitude, and $\hat{p}$ is the dimensionless pressure that remains after removing the hydrostatic component. In (1) $\tilde{\mathbf{C}}_g = (\tilde{c}, 0, -Ri_\tau \tilde{c}'')$ with $\tilde{c}'' = \tilde{c} - \tilde{c}^*$ where $\tilde{c}^*$ is the dimensionless concentration averaged over planes parallel to the bottom wall:

$$\tilde{c}^* = \frac{1}{L_x\, L_y} \int_0^{L_x} \int_0^{L_y} \tilde{c}\, dx\, dy \,. \tag{4}$$

Equations (1)-(3) apply to dilute non-cohesive sediment suspensions such that Boussinesq approximation holds and hindered settling can be neglected, and to suspension of particles sufficiently small such that inertial effects are of second order compared to settling effects (see section 3 of Cantero et al, 2008a; Ferry and Balachandar, 2001).

Variables with a tilde on top are dimensionless. The length scale employed is the channel half-height. The scale for concentration is the average volumetric concentration of sediment $\overline{c}^{(v)}$. The velocity scale is the average shear velocity defined as

$$u_{*,avg} = \left(\frac{\tau_t + \tau_b}{2\rho_w}\right)^{1/2} = \left(g \sin\theta\, R\, \overline{c}^{(v)} H/2\right)^{1/2} , \tag{5}$$

where τ_t and τ_b are the mean top and bottom wall shear stress, respectively, ρ_w is the density of the water, g is the magnitude of the gravity acceleration, and $R = (\rho_s - \rho_w)/\rho_w$ with ρ_s the density of the sediment particles. The time and pressure scales are thus the derived scales $T = h/u_{*,avg}$ and $\rho_w\, u_{*,avg}^2$, respectively.

The four dimensionless numbers in (1) and (3) are the Reynolds number, the Richardson number, the dimensionless settling velocity of the sediment particles, and the Schmidt number defined as

$$Re_\tau \equiv \frac{u_{*,avg}\, H/2}{\nu} = \frac{\left(g \sin\theta\, R\, \overline{c}^{(v)}\right)^{1/2} (H/2)^{3/2}}{\nu}\,, \tag{6}$$

$$Ri_\tau \equiv \frac{g \cos\theta\, R\, \overline{c}^{(v)} H/2}{u_{*,avg}^2} = \frac{1}{\tan\theta} \tag{7}$$

$$\tilde{V} \equiv \frac{V}{u_{*,avg}} = \frac{V}{\left(g \sin\theta\, R\, \overline{c}^{(v)} H/2\right)^{1/2}} \qquad \text{and} \tag{8}$$

$$Sc \equiv \frac{\nu}{\kappa}\,, \tag{9}$$

respectively, where ν is the kinematic viscosity of the water and κ is the diffusivity of the sediment particles. As explained in Cantero et al (2009a,b), the complex turbulence-sediment-wall interactions present in the proximity of the bottom boundary of real flows with rough wall are not central to the analysis of the present work and are lumped into a diffusivity model for the sediment particles. This diffusion of non-cohesive sediment particles arise from the long range hydrodynamics interactions between particles (Segre et al, 2001). The four parameters (6)-(9) define completely the problem in the TCR setting.

The channel walls are assumed to be smooth, and the sediment to be sufficiently fine so that there is no net deposition. Similar conditions are met when turbidity currents flow in bypass mode over a bedrock or coarse gravel bed (see for example Piper and Savoye, 1993; Gerber et al, 2008; Sequeiros et al, 2009). The following boundary conditions thus apply for the top and bottom walls

$$\tilde{\mathbf{u}} = 0 \qquad \text{at } \tilde{z} = 0 \text{ and } \tilde{z} = \tilde{H}, \tag{10}$$

$$\tilde{V} \cos\theta\, \tilde{c} + \frac{1}{Re_\tau\, Sc} \frac{\partial \tilde{c}}{\partial \tilde{z}} = 0 \qquad \text{at } \tilde{z} = 0 \text{ and } \tilde{z} = \tilde{H}, \tag{11}$$

while in the directions tangent to the walls periodic boundary conditions are applied for all variables. Although a no-slip condition is used in the present set of simulations, since the dominant physics of the problem mainly pertain to the interaction of turbulence generated at the bottom boundary with the self-stratification of the suspended sediment, the major conclusions to be drawn are insensitive to the precise nature of the top boundary condition. Recent simulations of particle-turbulence interaction in a turbidity current with free-slip condition on the top boundary have yielded results in close agreement with those using no-slip boundary condition (Shringarpure et al, 2012) and thus provide support for the relative insensitivity to the top boundary condition. Observe that the volume integral of (3) with the boundary conditions prescribed above reduces to $\mathrm{d}\tilde{c}^{(v)}/\mathrm{d}\tilde{t} = 0$. That is, as the flow evolves from the initial condition, the sediment particles are only redistributed within the channel. The total particle load of the flow is maintained constant and equal to the initial value ($\tilde{c}^{(v)} = 1$ for all times).

In this work mean variables are obtained by time-averaging the instantaneous horizontally averaged variables and are denoted by an overbar ($\bar{\cdot}$). Perturbations from the mean are denoted by a prime ($\cdot'$). For all cases considered the time of integration employed is over a dimensionless time interval of 50 units after the flow has achieved a statistically steady state. In comparison, the integral time scale for channel flow of $Re_\tau = 180$ has been reported to be $19.2\,\nu/u_*^2$ (see Quadrio and Luchini, 2003), that is approximately 0.1 dimensionless time units. The integration time is thus approximately over 455 integral time scales, and it has been checked to be long enough for the accurate computation of first and second order statistics.

3 Model for slope break and loss of lateral confinement

Consider a turbidity current flowing through a slope break as shown in figure 1a, or through a loss of lateral confinement as shown in figure 1b. The general case considered in this work is a change in flow configuration which is a combination of these two situations together. Upstream of the change in flow configuration the turbidity current flows in statistically steady state over an inclined bed that forms an angle θ_1 with respect to the horizontal direction. Some distance after the change in flow configuration, the turbidity current adjusts to the new regime and flows again in statistically steady state over an inclined bed that forms an angle θ_2 with respect to the horizontal direction.

This work addresses the characteristics of the flow in the far field of the change in flow configuration, where the immediate near-field influence of the break and/or the loss of lateral confinement themselves are not considered. The problem is thus idealized by considering two separated flows. These flows are modeled separately employing the TCR paradigm: TCR_1 and TCR_2 for the flows upstream and downstream of the change in flow configuration, respectively. Figure 1 shows schematically this setting for the cases of change in slope (a) and loss of lateral confinement (b). Conceptually, this model can be also thought as the time relaxation of the steady state solution corresponding to the TCR_1 setting to a new statistically steady state that corresponds to the TCR_2 settling.

When the flow transitions from the TCR_1 setting to the TCR_2 setting the only physical parameters that change are θ, H and $\overline{c}^{(v)}$ since g, R, ν, V and κ remain unaltered. With this in mind, the four dimensionless numbers that control the flow for the TCR_2 setting can be recast as

$$Re_{\tau,2} = Re_{\tau,1}\left(\frac{\sin\theta_2}{\sin\theta_1}\right)^{1/2}\left(\frac{\overline{c}_2^{(v)}}{\overline{c}_1^{(v)}}\right)^{1/2}\left(\frac{H_2}{H_1}\right)^{3/2}, \tag{12}$$

$$Ri_{\tau,2} = \frac{1}{\tan\theta_2}, \tag{13}$$

$$\tilde{V}_2 = \tilde{V}_1\left(\frac{\sin\theta_1}{\sin\theta_2}\right)^{1/2}\left(\frac{\overline{c}_1^{(v)}}{\overline{c}_2^{(v)}}\right)^{1/2}\left(\frac{H_1}{H_2}\right)^{1/2}, \quad \text{and} \tag{14}$$

$$Sc_2 = Sc_1, \tag{15}$$

which means that once the TCR_1 setting and the downstream slope (θ_2) are set, the TCR_2 problem has only two degree of freedom to be specified: $\overline{c}_2^{(v)}/\overline{c}_1^{(v)}$ and

H_2/H_1. These two degrees of freedom of the coupled system are employed to enforce conservation of mass.

3.0.1 Mass conservation enforcement

Transition from section 1 to section 2 is likely to involve complex non-stationary processes, which will not be directly simulated or addressed here. We consider sections 1 and 2 to be sufficiently upstream and downstream of the change of flow configuration. We assume that the net flow of both the carrier fluid and the particles are constant as the current transitions from section 1 to section 2. The conservation of suspended sediments between sections 1 and 2 is consistent with the concentration boundary conditions employed. Mass conservation for the mean flow between TCR_1 and TCR_2 is enforced by control volume analysis. Employing the control volume CV of figure 1 conservation of water mass implies

$$\int_0^{B_1}\int_0^{H_1} \rho_w \left(1-\overline{c}_1\right) \overline{u}_1 \mathrm{d}z\mathrm{d}y = \int_0^{B_2}\int_0^{H_2} \rho_w \left(1-\overline{c}_2\right) \overline{u}_2 \mathrm{d}z\mathrm{d}y\,, \tag{16}$$

where $\overline{u}_1$ and $\overline{u}_2$ are the mean water velocity at sections 1 and 2, respectively, $\overline{c}_1$ and $\overline{c}_2$ are the mean volumetric sediment concentration at sections 1 and 2, respectively, and B_1 and B_2 are the width of the channels at sections 1 and 2, respectively. Equation (16) can be recast as

$$H_1 B_1 u_{b1} \left(1-\chi_1 \overline{c}_1^{(v)}\right) = H_2 B_2 u_{b2} \left(1-\chi_2 \overline{c}_2^{(v)}\right) \tag{17}$$

where

$$u_b = \frac{1}{H\,B} \int_0^{B}\int_0^{H} \overline{u}\,\mathrm{d}z\mathrm{d}y \tag{18}$$

is the mean velocity and

$$\chi = \frac{1}{H\,B\,u_b\,\overline{c}^{(v)}} \int_0^{B}\int_0^{H} \overline{u}\,\overline{c}\,\mathrm{d}z\mathrm{d}y \tag{19}$$

is an $O(1)$ shape factor. Employing the assumption of dilute flow, i.e. $\overline{c}_1^{(v)} \ll 1$ and $\overline{c}_2^{(v)} \ll 1$ (17) can be simplified to

$$H_1\,B_1\,u_{b1} = H_2\,B_2\,u_{b2}. \tag{20}$$

Employing the same approach, conservation of sediment mass in CV implies

$$\int_0^{B_1}\int_0^{H_1} \rho_s \overline{c}_1 \left(\overline{u}_1 + V\sin\theta_1\right) \mathrm{d}z\mathrm{d}y = \int_0^{B_2}\int_0^{H_2} \rho_s \overline{c}_2 \left(\overline{u}_2 + V\sin\theta_2\right) \mathrm{d}z\mathrm{d}y. \tag{21}$$

Here the streamwise component of the diffusive flux of sediment has been neglected. This equation can be recast as

$$H_1 B_1 \overline{c}_1^{(v)} \left(\chi_1\,u_{b1} + V\sin\theta_1\right) = H_2 B_2 \overline{c}_2^{(v)} \left(\chi_2\,u_{b2} + V\sin\theta_2\right), \tag{22}$$

and simplified to

$$H_1 B_1 \overline{c}_1^{(v)} \chi_1 \, u_{b1} = H_2 B_2 \overline{c}_2^{(v)} \chi_2 \, u_{b2} \tag{23}$$

by means of the fact that $V \sin\theta_1 \ll u_{b1}$ and $V \sin\theta_2 \ll u_{b2}$.

A pseudo friction factor can be defined as

$$\gamma \equiv \frac{u_b}{u_{*,avg}} = \frac{u_b}{\left(g \sin\theta \, R \, \overline{c}^{(v)} \, H/2\right)^{1/2}}, \tag{24}$$

for each TCR setting. From (20) and (23)

$$\frac{\overline{c}_2^{(v)}}{\overline{c}_1^{(v)}} = \frac{\chi_1}{\chi_2}, \quad \text{and} \tag{25}$$

$$\frac{H_2}{H_1} = \left(\frac{\chi_2}{\chi_1}\right)^{1/3} \left(\frac{\gamma_1}{\gamma_2}\right)^{2/3} \left(\frac{B_1}{B_2}\right)^{2/3} \left(\frac{\sin\theta_1}{\sin\theta_2}\right)^{1/3}, \tag{26}$$

which are the values of $\overline{c}_2^{(v)}/\overline{c}_1^{(v)}$ and H_2/H_1 that enforce mass conservation between the two TCR settings.

4 Solution strategy

Once the TCR_1 setting is fixed the corresponding TCR_2 setting that enforces conservation of mass is completely defined by the following set of parameters

$$Re_{\tau,2} = Re_{\tau,1} \frac{B_1}{B_2} \frac{\gamma_1}{\gamma_2}, \tag{27}$$

$$Ri_{\tau,2} = \frac{1}{\tan\theta_2}, \tag{28}$$

$$\tilde{V}_2 = \tilde{V}_1 \left(\frac{B_2}{B_1}\right)^{1/3} \left(\frac{\sin\theta_1}{\sin\theta_2}\right)^{1/3} \left(\frac{\gamma_2}{\gamma_1}\right)^{1/3} \left(\frac{\chi_2}{\chi_1}\right)^{1/3} \quad \text{and} \tag{29}$$

$$Sc_2 = Sc_1. \tag{30}$$

Observe that the values of χ and γ are stationary steady state values and, consequently, χ_2 and γ_2 are only known once the stationary state solution of TCR_2 has been computed. The TCR_2 solution requires thus an iterative process:

- Set $\gamma_2^{(0)} = \gamma_1$, $\chi_2^{(0)} = \chi_1$
- Loop until convergence, $i = 1$
  - compute $Re_{\tau,2}^{(i)} = Re_{\tau,1} \frac{\gamma_1 \, B_1}{\gamma_2^{(i-1)} \, B_2}$
  - compute $\tilde{V}_2 = \tilde{V}_1 \left(\frac{\gamma_2^{(i-1)} \, \chi_2^{(i-1)} \, B_2 \, \sin\theta_1}{\gamma_1 \, \chi_1 \, B_1 \, \sin\theta_2} \right)^{1/3}$
  - solve $\mathrm{TCR}_2^{(i)}$
  - compute $\gamma_2^{(i)}$ and $\chi_2^{(i)}$
  - convergence if $|\gamma_2^{(i)} - \gamma_2^{(i-1)}| \leq \mathrm{TOL}_\gamma$ and $|\chi_2^{(i)} - \chi_2^{(i-1)}| \leq \mathrm{TOL}_\chi$
  - i=i+1.

It is worth mentioning that the solution of each $\mathrm{TCR}_2^{(i)}$ problem demands $O(10^5)$ time iterations to reach statistically steady state and another $O(10^5)$ time iterations in order to compute converged statistics.

The dimensionless governing equations are solved using a de-aliased pseudospectral code (Canuto et al, 1988). Fourier expansions are employed for the flow variables in the horizontal directions $(x - y)$, and a Chebyshev expansion with Gauss-Lobatto quadrature points is employed in the inhomogeneous vertical direction (z). The grid resolution used is $N_x = 96 \times N_y = 96 \times N_z = 97$ and the nonlinear terms are computed in a grid $3N_x/2 \times 3N_y/2 \times N_z$ in order to prevent aliasing errors. This grid assures that the energy of the high wave number modes is several orders of magnitude smaller than the energy of the low wave number modes (see Figure 3 in Cantero et al, 2009a). An operator splitting method is used to solve the momentum equation along with the incompressibility condition (see for example Brown et al, 2001). A low-storage mixed third order Runge-Kutta and Crank-Nicolson scheme is used for the temporal discretization of the advection-diffusion terms, with a pressure correction applied at the end of each stage. More details on the implementation of this numerical scheme can be found in Cortese and Balachandar (1995). Validation of the code can be found in Cantero et al (2007a, 2008c, 2009a).

5 Application of the model

This section reports results on the application of the model to two different situations: turbidity currents driven by fine and coarser sediment flowing through a decreasing slope. Here the distinction between the definitions of fine and coarse sediments is as follows. In the case of fine sediment after the reduction in the slope of the channel the flow still remains turbulent, with only a modest influence on the turbulence statistics. Whereas, in case of coarse sediments, after the change in slope, turbulence is totally suppressed. The before and after slope break simulations performed to address these two situations are reported in Table 1. Intermediate simulations in the transition process during convergence are not reported. In obtaining the results for FLS and CLS in Table 1 the tolerances TOL_γ and TOL_χ have been set to 0.05, and 7 and 6 iterations were needed, respectively. The present analysis focuses on the effect of slope change on the flow and thus the channel width is kept a constant, i.e. the simplification of $B_2/B_1 = 1$ has been employed. As indicated in section 3, B_2/B_1 is a fixed parameter in the model.

The analysis is performed for a typical field scale turbidity current of height $H = 20$m running on a slope $\theta_1 = 5^\circ$ with a mean volume concentration $\overline{c}_1^{(v)} = 0.005$ of sand particles (in water: $R = 1.65$ and $\nu = 10^{-6}$ m^2/s). From (5) $u_{*,avg,1} = 0.27$ m/s for this case. Two different sediment sizes are considered: a *fine* sediment with diameter $d = 40$ μm with settling velocity of $V = 1.4$ mm/s (García, 2008), and a *coarse* sediment with diameter $d = 60$ μm with settling velocity of $V = 3.1$ mm/s (García, 2008). The corresponding dimensionless settling velocities are $\tilde{V} = 5.4 \times 10^{-3}$ and $\tilde{V} = 1.2 \times 10^{-2}$ for the *fine* and *coarse* sediments, respectively. Owing to computational resource limitation it will not be possible to perform DNS at very large Reynolds numbers typical of real turbidity currents. In this work the simulations are performed for a modest Reynolds number of $Re_{\tau,1} = 180$. This value of $Re_{\tau,1}$ corresponds to a value of $Re_{b,1} = u_{b1}H_1/2\nu \sim 3000$, i.e. in the

turbulent regime. Extrapolation to large Reynolds number flows can be found in Cantero et al (2012). In both cases the current is assumed to transition to a lower slope of $\theta_2 = 2^\circ$.

Table 2 presents the results for the final stationary steady state of the flow after the change of slope. Both situations, fine- and coarse-sediment driven currents, show an increase of the current height for the lower slope. The averaged volume concentration remains practically unchanged after the flow transition owing to the enforced boundary condition for $\tilde{c}$. The change of 5% reported for case C in Table 2 owes more likely to the approximation of dilute flow employed in writing (20). The pseudo friction factor γ shows an increase for both cases.

Figure 2 presents the mean concentration wall-normal profiles. Figure 2a shows the results corresponding to the fine-sediment driven current, while 2b shows the results corresponding to the coarse-sediment driven current. A clear increase in the concentration can be seen in the bottom half of the channel for both cases as the currents transitions to the low slope. The increase is larger for the case of coarse sediment showing lager concentration gradients and thus stronger stratification of the flow. For the case of fine sediment the increase of concentration in the bottom half is minor and there is only a weak change in the concentration gradients.

The effects of stratification are clearly seen in the wall-normal profiles of streamwise velocity shown in figure 3. Figure 3a shows the results corresponding to the fine-sediment driven current, while 3b shows the results corresponding to the coarse-sediment driven current. Less turbulent mixing of momentum is expected for the stronger stratified flows and this is evident in figure 3b, which shows larger velocity gradients in the bottom half of the channel. The velocity profile corresponding to the fine-sediment driven current (3a) flowing over the low slope show minor changes and weak evidence of stratification effects.

A measure of the level of turbulence in the flow can be obtained from the turbulent kinetic energy (TKE)

$$k = \frac{1}{2}\left(\overline{u'^2} + \overline{v'^2} + \overline{w'^2}\right), \tag{31}$$

where $u_i' = u_i - \overline{u_i}$ is the perturbation from the mean. Figure 4a shows the results corresponding to the fine-sediment driven current and 4b shows the results corresponding to the coarse-sediment driven current. The effect of change in slope in the TKE is negligible for the case of the fine-sediment driven current. For the case of the coarse-sediment driven current, on the other hand, the effect is strong and the peak of TKE has dramatically reduced to about 10% of the peak value observed in the high slope flow regime.

Finally, the ability of the flow turbulence to mix momentum and mass in the vertical can be measured by the ratio between the corresponding turbulent fluxes and viscous fluxes

$$\frac{\tau_{Re}}{\tau_{vis}} = \frac{-\overline{u'w'}}{\nu \mathrm{d}\overline{u}/\mathrm{d}z} \qquad \text{and} \qquad \frac{F_{Re}}{F_{vis}} = \frac{-\overline{w'c'}}{\kappa \mathrm{d}\overline{c}/\mathrm{d}z}, \tag{32}$$

respectively. Figures 5 shows the ratio between the Reynolds stress and viscous stress, and figure 6 shows the ratio between the concentration turbulent fluxes and viscous fluxes. Frames (a) correspond to the fine-sediment driven current and they show a minor decreases in the ability to mix momentum and mass. Frames (b)

that correspond to the coarse sediment driven current, on the other hand, show no turbulent mixing in the bottom half of the channel.

The results reported in this work have focused on a set-up where bottom slope of the channel changes and have considered the situation of uniform channel width (i.e., $B_2/B_1 = 1$). A similar investigation can be considered where the bottom slope is held fixed, while the channel width is increased. It can be clearly seen from (27) and (29) that any reduction of lateral confinement ($B_2/B_1 > 1$) reduces $Re_{\tau,2}$ and increases $\tilde{V}_2$ by a fixed factor, thus augmenting the effect of turbulence damping by stratification. Thus, abrupt and total suppression of turbulence can be expected for situations of rapidly increase in the spanwise extent of the current, if this reduction in lateral confinement is above a certain threshold (Cantero et al, 2009a).

6 Conclusions

This work presents a simplified model for the direct numerical simulation of continuous turbidity currents with focus on addressing turbulence modulation. The model extends the turbidity current with a roof model of Cantero et al (2009a) for the analysis of slope breaks and loss of lateral confinement. The analysis is implemented with two separate simulations for sections upstream and downstream of the change of flow configurations, and connected by imposing mass conservation of water and suspended sediment.

Suspended sediment plays a dual role in turbidity currents. On one hand, it drives the flow through its influence on the streamwise component of the momentum equations. On the other hand, it stratifies the flow by its influence on the wall-normal component of the momentum equations. The parameter that measures the relative importance of these two effects in the momentum equations is the Richardson number, which for the case of turbidity currents is directly related to the slope ($Ri_\tau = 1/\tan\theta$). Thus, as the bed slope decreases, stratification effects become stronger. The other important parameter that mediates stratification effects is the dimensionless settling velocity of the suspended sediment ($\tilde{V}$), which indirectly measures suspended sediment concentration gradients. Thus sediments with larger settling velocity induce larger concentration gradients.

The model developed in this work has been employed to analyze turbulence modulation in turbidity currents owing to changes on the bed slope. The analysis has been performed for turbidity currents flowing from a slope $\theta_1 = 5^\circ$ to a lower slope $\theta_2 = 2^\circ$, and driven by two different sediments sizes. In the first case the turbidity current is driven by the finer sediment. The flow undergoes minor modifications and remains fully turbulent after the change in bed slope. In the second case the turbidity current is driven by the coarser sediment. As opposed to the first case, the flow suffers major changes. Large concentration gradients develop and strongly stratify the flow. Turbulence is totally suppressed, suspended sediment rains out and the flow eventually ceases to exist.

This work focus on flows driven by granular non-cohesive particles, and the effects on turbulence modulation reported herein are due to stratification effects. There are other mechanisms of turbulence suppression. For example, Baas and Best (2002) present turbulence modulation due to rheology effects. In the present simulations we do not observe definite layers in the flow and the formation of

Kelvin-Helmholtz instabilities do not develop in the current as reported by Baas and Best (2002).

Furthermore, real turbidity currents are polydisperse. Their response to slope changes would be a combination of the two cases analyzed in this work, mediated by the relative concentration of fine over coarse sediment.

Mariano I. Cantero gratefully acknowledges the support from CONICET, CNEA and ANPCyT through PICT-2010-2459. We gratefully acknowledge the support from Shell International Exploration and Production and from the National Center for Supercomputing Applications (NCSA) at the University of Illinois at Urbana-Champaign (UIUC). The participation of Gary Parker in this research was made possible by the National Center for Earth Surface Dynamics (NCED), a Science and Technology Center funded by the U.S. National Science Foundation. S. Balachandar acknowledges support from National Science Foundation through the grants OCE-1131016 and OISE-0968313,

References

Allen J (1985) Principles of Physical Sedimentology. George Allen and Unwin Ltd., London, UK, 272 pages

Amy L, Hogg A, Peakall J, Talling P (2005) Abrupt transitions in gravity currents. Journal of Geophysical Research 110:F03,001, doi:10.1029/2004JF000,197

Armenio V, Sarkar S (2002) An investigation of stably stratified turbulent channel flow using large-eddy simulation. Journal of Fluid Mechanics 459:1–42

Baas J, Best J (2002) Turbulence modulation in clay-rich sediment-laden flows and some implications for sediment deposition. Journal of Sedimentary Research 72(3):336–340

Brown D, Cortez R, Minion M (2001) Accurate projection methods for the incompressible navier-stokes equations. Journal of Computational Physiscs 168:464–499

Cantero M, Balachandar S, García M (2007a) Highly resolved simulations of cylindrical density currents. Journal of Fluid Mechanics 590:437–469

Cantero M, Lee JR, Balachandar S, García M (2007b) On the front velocity of gravity currents. Journal of Fluid Mechanics 586:1–39

Cantero M, Balachandar S, García M (2008a) An eulerian-eulerian model for gravity currents driven by inertial particles. International Journal of Multiphase Flow 34:484–501

Cantero M, Balachandar S, García M, Bock D (2008b) Turbulent structures in planar gravity currents and their influence of the flow dynamics. Journal of Geophysical Research - Oceans 113:C08,018

Cantero M, García M, Balachandar S (2008c) Effect of particle inertia on the dynamics of depositional particulate density currents. Computers and Geosciences 34:1307–1318

Cantero M, Balachandar S, Cantelli A, Pirmez C, Parker G (2009a) Turbidity current with a roof:direct numerical simulation of self-stratified turbulent channel flow driven by suspended sediment. Journal of Geophysical Research - Oceans 114:C03,008

Cantero M, Balachandar S, Parker G (2009b) Direct numerical simulation of stratification effects in a sediment-laden turbulent channel flow. Journal of Turbulence 10(27):1–28

Cantero MI, Cantelli A, Pirmez C, Balachandar S, Mohrig D, Hickson TA, Yeh Th, Naruse H, Parker G (2012) Emplacement of massive turbidites linked to extinction of turbulence in turbidity currents. Nature Geosci 5(1):42–45, URL http://dx.doi.org/10.1038/ngeo1320

Canuto C, Hussaini M, Quarteroni A, Zang T (1988) Spectral Methods in Fluid Dynamics. Springer-Verlag, New York, 557 pages

Cortese T, Balachandar S (1995) High performance spectral simulation of turbulent flows in massively parallel machines with distributed memory. International Journal of Supercomputer Applications 9(3):187–204

Ferry J, Balachandar S (2001) A fast eulerian method for disperse two-phase flow. International Journal of Multiphase Flows 27:1199–1226

García M (1992) Turbidity currents. In: Brekhovskikh L, Turekian K, Emery K, Tseng C (eds) Encyclopedia of Earth System Science, vol 4, Academic Press, Inc., New York, pp 399–408

García M (ed) (2008) Manual 110. Sedimentation engineering: processes, measurements, modeling and practice, American Society of Civil Engineering (ASCE), Reston, VA, USA, p 1150

Gerber T, Pratson L, Wolonsky M, Steel R, Mohr J, Swenson J, Paola C (2008) Clinoform progradation by turbidity currents: modeling and experiments. Journal of Sedimentary Research 78:220–238

Härtel C, Meiburg E, Necker F (2000) Analysis and direct numerical simulation of the flow at a gravity-current head. Part 1. Flow topology and front speed for slip and no-slip boundaries. Journal of Fluid Mechanics 418:189–212

Necker F, Härtel C, Kleiser L, Meiburg E (2005) Mixing and dissipation in particle-driven gravity currents. Journal of Fluid Mechanics 545:339–372

Piper D, Savoye B (1993) Processes of late quaternary turbidity current flow and deposition on the Var deep-sea fan, north-west Mediterranean Sea. Sedimentology 40:557–582

Pirmez C, Imran J (2003) Reconstruction of turbidity currents in amazon channel. Marine and Petroleum Geology 20:823 – 849

Quadrio M, Luchini P (2003) Integral space-time scales in turbulent wall flows. Physics of Fluids 15(8):2219–2227

Segre PN, Liu F, Umbanhowar P, Weitz DA (2001) An effective gravitational temperature for sedimentation. Nature 409:594–597

Sequeiros OE, Naruse H, Endo N, Garcia MH, Parker G (2009) Experimental study on self-accelerating turbidity currents. J Geophys Res 114, DOI 10.1029/2008JC005149

Shringarpure M, Cantero MI, Balachandar S (2012) Dynamics of complete turbulence suppression in turbidity currents driven by monodisperse suspensions of sediment. Journal of Fluid Mechanics 712:384–417

Stacey M, Bowen A (1988a) The vertical structure of density and turbidity currents: theory and observations. Journal of Geophysical Research 93:3528–3542

Stacey M, Bowen A (1988b) The vertical structure of turbidity currents and a necessary condition for self-maintenance. Journal of Geophysical Research 93:3543–3553

Table 1 Cases studied in this work. For all cases the domain size is $L_x = 2\pi H \times L_y = 2\pi H/3 \times L_z = H$, and resolution is $N_x = 96 \times N_y = 96 \times N_z = 97$. FHS refers to the simulation corresponding to fine sediment and high slope, FLS refers to the simulation corresponding to fine sediment and low slope, CHS refers to the simulation corresponding to coarse sediment and high slope, and CLS refers to the simulation corresponding to coarse sediment and low slope. For the cases of low slope simulations the reported values correspond the the final values after convergence of the algorithm for mass conservation.

Case	θ	$\tilde{V}$	Re_τ
FHS	5	5×10^{-3}	180
FLS	2	6.87×10^{-3}	173
CHS	5	10^{-2}	180
CLS	2	1.41×10^{-2}	153

Table 2 Results for cases studied in this work. For all cases $B_2/B_1 = 1$. F refers to the model applied to fine sediment, and C refers to the model applied to coarse sediment.

Case	χ_1	χ_2	γ_1	γ_2	H_2/H_1	$\overline{c}_2^{(v)}/\overline{c}_1^{(v)}$
F	0.9998	0.9992	15.6	16.3	2.43	1.00
C	0.9990	0.9548	15.9	18.7	2.21	1.05

Talling PJ, Wynn RB, Masson DG, Frenz M, Cronin BT, Schiebel R, Akhmetzhanov AM, Dallmeier-Tiessen S, Benetti S, Weaver PPE, Georgiopoulou A, Zuhlsdorff C, Amy LA (2007) Onset of submarine debris flow deposition far from original giant landslide. Nature 450(7169):541–544, DOI 10.1038/nature06313, URL http://dx.doi.org/10.1038/nature06313

Turner J (1973) Buoyancy Effects in Fluids. Cambridge University Press

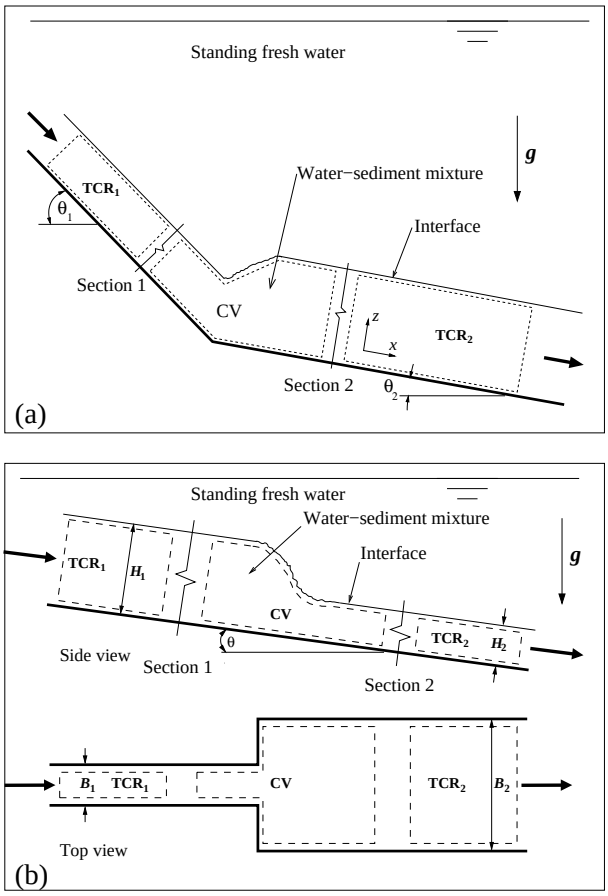

Fig. 1 Problem setting. a: Conceptualization of slope break. b: Conceptualization of loss of lateral confinement. The transitions between sections 1 and 2 are not necessarily sudden changes, but could actually be smooth changes in slope and/or width of the confining channel.

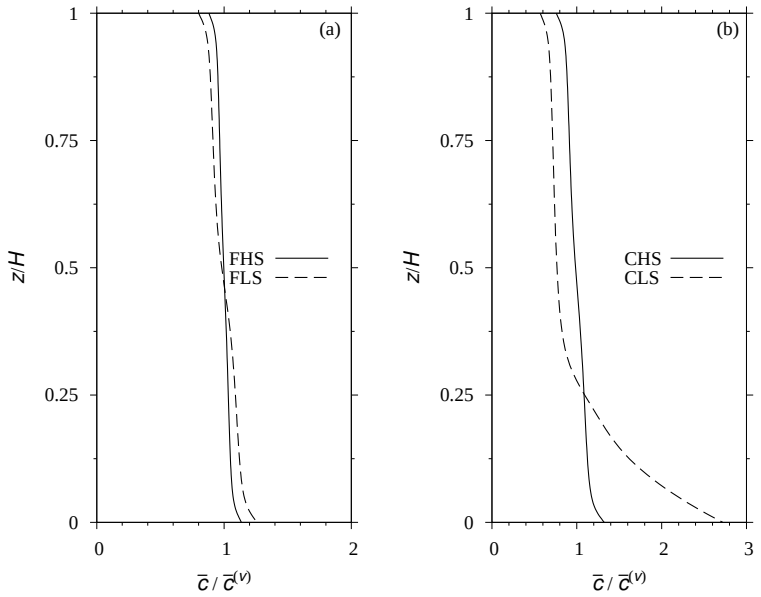

Fig. 2 Mean concentration profiles. Frame a: fine sediment, and frame b: coarse sediment.

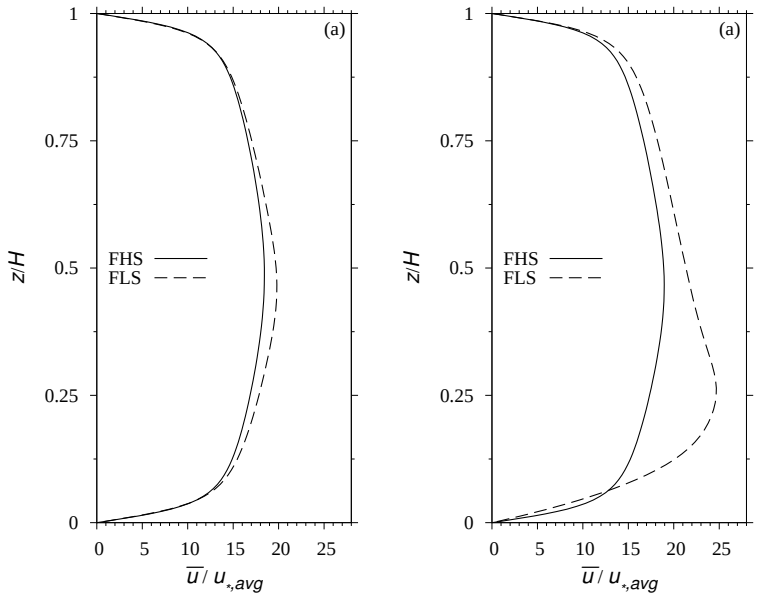

Fig. 3 Mean velocity profiles. Frame a: fine sediment, and frame b: coarse sediment.

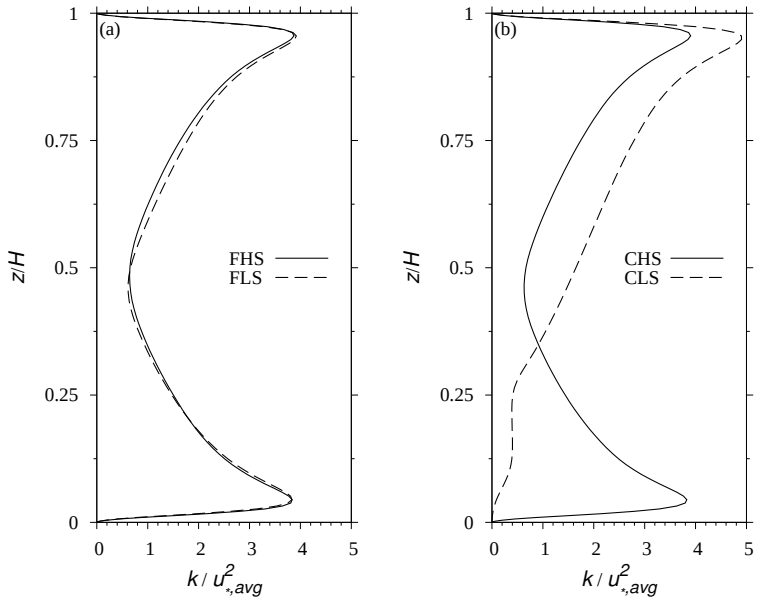

Fig. 4 Turbulent kinetic energy profiles. Frame a: fine sediment, and frame b: coarse sediment.

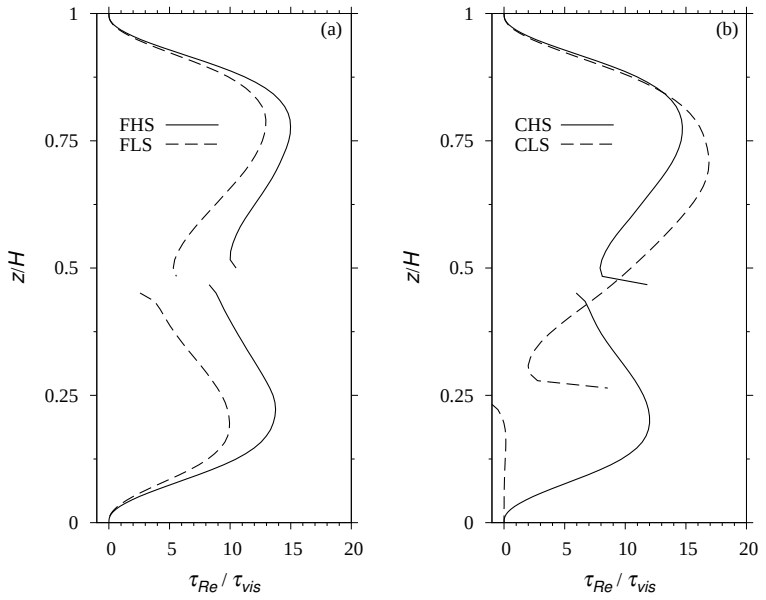

Fig. 5 Reynolds to viscous stress ratio. Frame a: fine sediment, and frame b: coarse sediment.

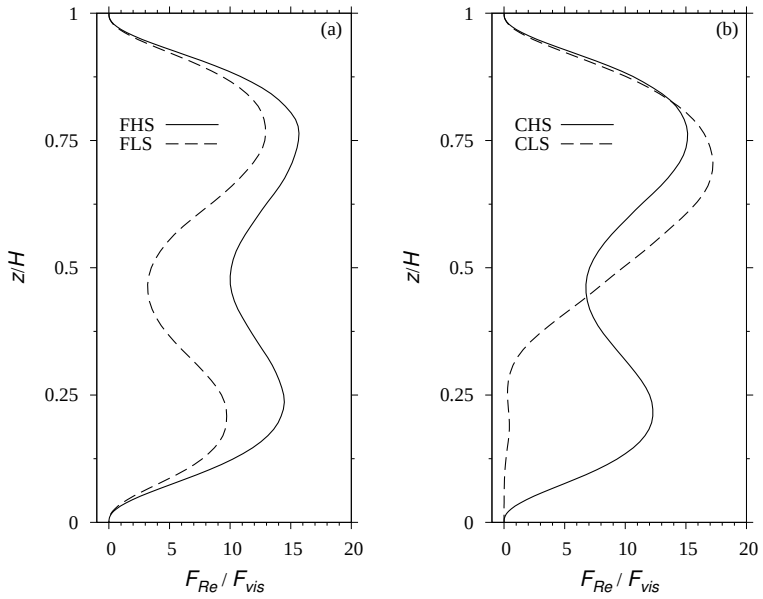

Fig. 6 Turbulent to viscous fluxes ratio. Frame a: fine sediment, and frame b: coarse sediment.